Available online at www.sciencedirect.com
ScienceDirect
C. R. Physique 9 (2008) 379–388
COMPTES RENDUS PHYSIQUE
http://france.elsevier.com/direct/COMREN/

Materials subjected to fast neutron irradiation/Matériaux soumis à irradiation par neutrons rapides

The Fe–Cr system: atomistic modelling of thermodynamics and kinetics of phase transformations

Duc Nguyen-Manh *, M.Yu. Lavrentiev, Sergei L. Dudarev

EUROATOM/UKAEA Fusion Association, Culham Science Centre, Abingdon, OX14 3DB, United Kingdom

Available online 3 March 2008

Abstract

To understand the behaviour of irradiated defects and kinetic pathways of micro-structural evolution in Fe–Cr alloys, we use a combination of density functional theory with statistical approaches involving cluster expansions and Monte Carlo simulations. A lowest negative mixing enthalpy is found at 6.25% Cr that is consistent with our DFT prediction of an ordered $Fe_{15}Cr$ structure. At 50% Cr, it is found that the predicted enthalpy of formation is 4 times smaller than that calculated by the CPA approach. Thermodynamic and precipitation properties are then discussed in term of segregation between the $Fe_{15}Cr$ and α'-Cr phases and of vacancy-mediated kMC simulation. ***To cite this article: D. Nguyen-Manh et al., C. R. Physique 9 (2008).***

Résumé

Le système de Fe–Cr : modélisation atomique des propriétés thermodynamiques et cinétiques de transfomations des phases. Pour comprendre les propriétés des défauts d'irradiation et les cinétiques d'évolution des microstructures des alliages Fe–Cr, nous utilisons la théorie de la fonctionnelle de la densité combinée à des approches statistiques de type développement d'amas et Monte Carlo. L'énergie de mélange du système Fe–Cr présente un minimum pour une teneur en Cr de 6,25 %, ce qui est en accord avec la prédiction des calculs de la structure ordonnée $Fe_{15}Cr$, basés sur la fonctionnelle de la densité. Pour une teneur de 50 % en Cr, on trouve une enthalpie de formation qui est quatre fois plus petite que celle calculée dans l'approche CPA. Nous discutons les propriétés thermodynamiques et la précipitation dans le système Fe–Cr en terme de séparation des phases Fe15Cr et α' riche en Cr, simulée par Monte Carlo cinétique basée sur un mécanisme lacunaire de diffusion. ***Pour citer cet article : D. Nguyen-Manh et al., C. R. Physique 9 (2008).***

Keywords: Fe–Cr alloys; Thermodynamics; Kinetics

Mots-clés : Alliages Fe–Cr ; Thermodynamiques ; Kinétiques

1. Introduction

Fe–Cr alloys form the basis of many industrially important steels. Ferritic/martensitic steels with 7–12 wt% Cr are candidates for the internal structures of future fusion power plants because of their remarkable resistance to swelling, and their adequate mechanical properties (tensile, impact and creep resistance up to 550 °C) [1,2]. At the same time

* Corresponding author.
E-mail address: duc.nguyen@ukaea.org.uk (D. Nguyen-Manh).

1631-0705/$ – see front matter
doi:10.1016/j.crhy.2007.10.011

these steels suffer from radiation hardening and embrittlement below 400 °C even at moderate irradiation doses. In order to facilitate the use of these steels, it is therefore necessary to understand the factors driving the evolution of microstructure, which is linked to the degradation of mechanical properties, and to access their structural stability during neutron irradiation or long thermal aging. It is in the context of this research programme that binary Fe–Cr alloys are studied as a model system, from which the fundamental mechanisms of radiation damage can be investigated and quantified.

Understanding the behaviour of the Fe–Cr system represents a considerable challenge for modelling since magnetic interactions involving both constituting elements of the alloy give rise to a fairly complex picture of interatomic interactions. Furthermore, since iron, chromium and the Fe–Cr binary system all form bcc crystal structures, we note an interesting electronic structure aspect of the behaviour of this system that has significant implications for the development of inter-atomic potentials [3–5]. The available experimental information on the phase diagram of the binary Fe–Cr only covers the range of relatively high temperature where the alloy forms a bcc solid solution. The situation at low temperature is less certain, in particular with regard to the magnetic properties of Fe–Cr alloys considered as a function of Cr concentration. Most of the modelling studies of Fe–Cr alloys were based, until very recently, on the work by Olsson et al. [6] that demonstrated that this alloy exhibits unusual thermodynamic behaviour at low temperatures. By using an ab initio-based coherent potential approximation (CPA), or, in other words, the mean field theory approximation for a substitutional random alloy, the authors of Ref. [6] showed that the mixing enthalpy versus Cr concentration curves in the ferromagnetic state exhibit a sign change. The mixing enthalpy is negative in the Fe-rich region and becomes positive above a certain critical level of chromium concentration close to 10%, with a relatively high and broad maximum at 50% Cr. The CPA calculations have raised two important questions. On the one hand, they showed that the conventional phase diagram of the Fe–Cr alloy was probably not fully consistent with the negative sign of the mixing enthalpy in the Fe-rich region where Cr is easily dissolved in iron. On the other hand, the recently developed inter-atomic potentials for the Fe–Cr system that use information from the CPA database, showed that there were discrepancies between short-range order parameters predicted by the model and observed experimentally, raising "*doubts in the accuracy of ab initio predictions*" [7].

In this study, we re-examine the binary alloy phase diagram by going beyond the mean-field CPA treatment and by using the cluster expansion (CE) technique based on a full ab initio database. This database contains information derived from the DFT spin-polarized total-energy calculations performed for binary Fe–Cr alloys across the entire range of chromium concentrations. We then use the exchange Monte Carlo technique to investigate the effects of phase separation in bcc Fe–Cr alloys for various Cr concentrations and for various temperatures. Finally, by using the activation energies for vacancy migration derived from DFT calculations, we study the dynamics of precipitation of Cr clusters via vacancy-mediated kinetic Monte Carlo (kMC) simulations.

2. The enthalpy of mixing of the Fe–Cr system

In the cluster expansion formalism the configuration formation enthalpy of an alloy is mapped exactly on a set of multi-site interaction parameters $\{J\}$ of an Ising-like Hamiltonian:

$$H_{\mathrm{CE}}\big(\{\sigma\}\big) = J_0 + \sum_i J_i\sigma_i + \sum_{i<j} J_{ij}\sigma_i\sigma_j + \sum_{i<j<k} J_{ijk}\sigma_i\sigma_j\sigma_k + \cdots \tag{1}$$

For a binary system, the occupation variable $\{\sigma\}$ indicates whether a lattice site is occupied by an atom of type A or B, respectively. Because of the very small lattice mismatch between bcc-Fe and bcc-Cr, we did not include the contribution from constitutional strain energy in the Hamiltonian. In principle, it can be considered in a general CE formalism [8]. The CE interaction coefficients $\{J\}$ can be obtained either from an unconstrained [9] or a constrained [10] fit to a DFT database. Fig. 1 shows the enthalpy of mixing for the binary Fe–Cr system found by annealing exchange Monte Carlo simulation for a $4 \times 4 \times 4$ supercell in the CE approximation [11]. These data are compared with those from a DFT database constructed by means of extensive spin-polarized calculations performed using the VASP code [12,13]. A new finding derived from this study is that both DFT and exchange Monte Carlo simulations predict the formation of an ordered structure at 6.25% Cr shown in Fig. 2. CE simulations show that the mixing enthalpy for 50% Cr alloy is 4 times smaller than that predicted by the CPA approach [6] ($\sim$20 meV/atom in CE simulations versus $\sim$80 meV/atom in CPA). In order to understand the origin of this difference, we evaluated the enthalpy of mixing for a homogeneous random configuration in the so-called Bragg–Williams approximation (BWA),

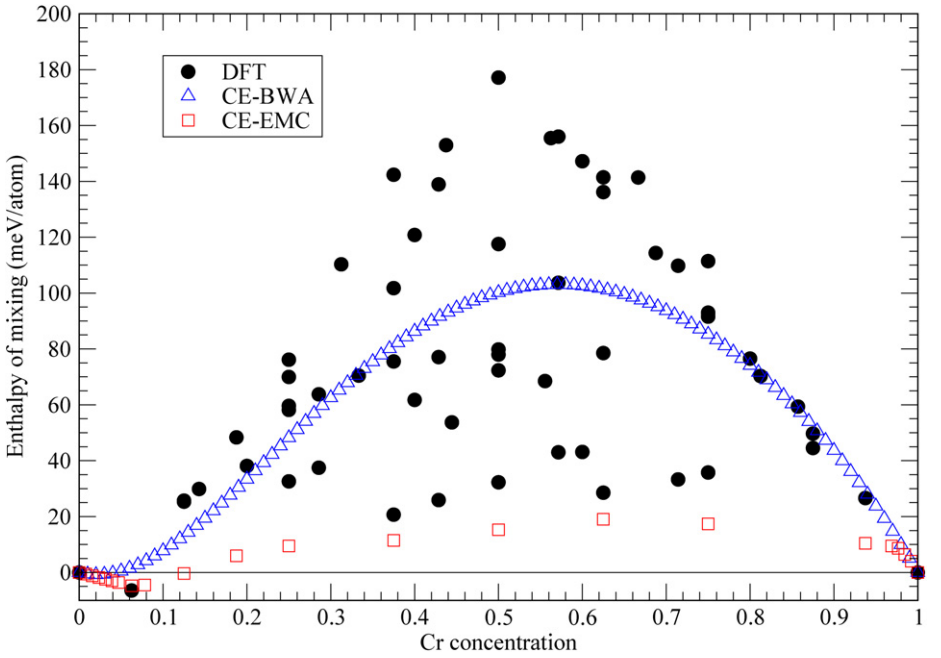

Fig. 1. Enthalpy of formation for Fe–Cr predicted by spin-polarized DFT calculations (black dots) [12], by simulated annealing of $4 \times 4 \times 4$ bcc supercells in the CE calculations (open square) [11] and by single-site cluster or the Bragg–Williams approximation (open triangles).

Fig. 1. Prédiction de l'enthalpie de formation de l'alliage Fe–Cr par calculs basés sur la fonctionnelle de la densité avec polarisation de spins (cercles pleins) [12], par la simulation du recuit de supercellules ($4 \times 4 \times 4$) cubiques centrées (carrés) et dans le cadre de l'approximation de point ou de Bragg–Williams (triangles).

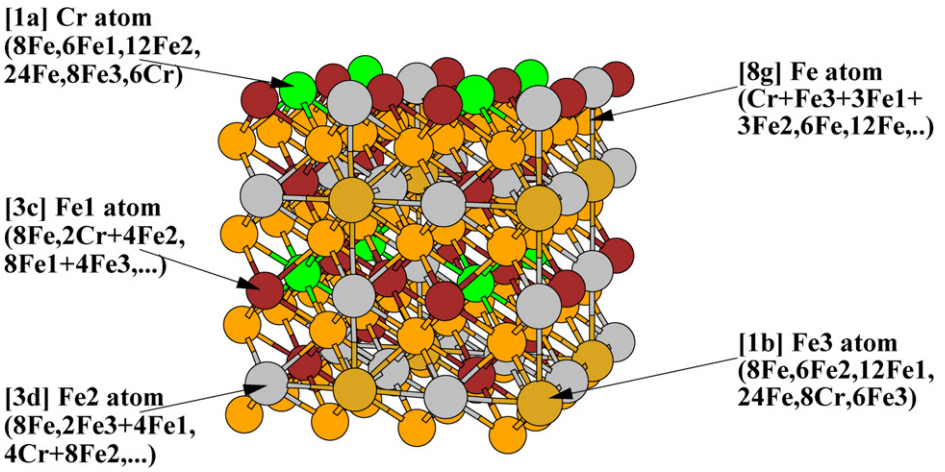

Fig. 2. Crystal structure of $Fe_{15}Cr$ predicted as the most stable phase in Fe-rich region by the present DFT and MC calculations, and presented in the form of a $2 \times 2 \times 2$ unit cell with 5 different crystallographic sites.

Fig. 2. Structure cristalline du composé ordonné $Fe_{15}Cr$. Les calculs basés sur la fonctionnelle de la densité et la méthode de Monte Carlo présentés dans ce papier montrent que ce composé est la phase la plus stable de la région riche en fer du diagramme Fe–Cr. La figure montre une cellule unitaire avec cinq sites cristallographiqes différents.

where the many-body correlations are approximated by single-site clusters [14]. Using the set of CE coefficients published in Table 1 of [11] and denoting the Cr concentration as x, Eq. (1) can be approximated by:

$$E_{\mathrm{BWA}}(x) = 59.11 + 82.2x - 145.12(1-2x)^2 + 7.92(1-2x)^3 + 44.91(1-2x)^4 + 33.18(1-2x)^5 \qquad (2)$$

The curve described by Eq. (2) is also plotted in Fig. 1. We find that the behaviour of mixing enthalpy predicted by Eq. (2) is comparable with that predicted by the CPA calculations [6]. By using the BWA for random solution and our CE coefficients, we recover the CPA results, and therefore confirm the validity of the present CE approach.

One of the main advantages of using the CE approximation over CPA is its ability to provide correct atomic configurations for the Fe–Cr system at different concentrations, for which subsequent electronic structure investigation can be performed [12]. We have shown that there is a strong variation of magnetic moment on the Cr site from $-1.7\mu_B$ in the solid solution limit in the Fe-rich region compared with $\pm 0.6\mu_B$ obtained for pure anti-ferromagnetic chromium in bcc structure. It has been also found that the dependence of the calculated spin-density treated as a function of composition that clustering of Cr has magnetic origin, which is particularly evident for alloys with a concentration higher than 10% Cr [12].

3. Magnetic properties of the ordered phase

The occurrence of the ordered $Fe_{15}Cr$ structure shown in the previous section has important implications in the interpretation of the Fe–Cr phase diagram in the low temperature limit, and in understanding segregation and precipitation in the Cr-rich region. The latter is conventionally interpreted from the experimental Fe–Cr phase diagram at high temperatures as the effect of phase separation between 'symmetrical' α (bcc-Fe) phase and α' (bcc-Cr) phases [15]. Our results show that in the low temperature region, the lowest negative enthalpy of mixing at 6.25% Cr and the presence of the ordered $Fe_{15}Cr$ phase give rise to the asymmetry of α–α' separation. Even at $T = 800$ K, the enthalpy of mixing remains negative for a range of concentration below 10% Cr (see Fig. 4 of Ref. [11]). The formation of an ordered phase with the lowest negative enthalpy of mixing provides an alternative approach for understanding the Fe–Cr phase diagram in comparison with previous theoretical studies starting from homogenous random treatment of alloy, using either the CPA formalism [6], the generalized perturbation approximation (GPA) to the CPA [16] or recently the so-called special quasirandom structures (SQS) with a supercell including disorder [17,18]. As we have demonstrated recently, the stabilization of long-ranged ordered $Fe_{15}Cr$ phase is determined by the lowest density of states (DOS) of the minority-spin channel at Fermi energy [19] that is in variance with a conventional argument on the correlation between phase stability and total DOS using for interpreting both CPA and SQS configurations [18].

Spin-polarized electronic structure calculations of the density of states (DOS) performed using a collinear approximation are shown in Fig. 3 for various crystallographic sites highlighted in Fig. 2. Analysis of the local DOS plots shows that a Cr atom (with magnetic moment of $-1.7\mu_B$) surrounded by only Fe atoms up to the fifth nearest neighbour (NN) shells, has its moment aligned anti-ferromagnetically in comparison with the ferromagnetically aligned moments associated with all the Fe sites. For the latter, the shape of local DOS is slightly different to those in pure bcc-Fe due to the different environments of various Fe atoms.

It is desirable to investigate the effect of non-collinear magnetism in Fe–Cr alloys because it would provide a direct match to experimental measurements of magnetic and structural changes as a function of Cr concentration. This can be done, for example, using the VASP code with the non-collinear magnetic option and taking into account spin–orbit coupling [20]. Table 1 shows the calculated magnetic properties found from self-consistent DFT calculations within non-collinear magnetism for the ordered $Fe_{15}Cr$ structure. The table gives averaged values for the spin and orbital moments for different atoms belonging to crystallographically equivalent sites in the $Fe_{15}Cr$ structure together with the ratios of these moments. The ratios vary between 0.0235 and 0.0243 depending on the symmetry of a Fe site. Comparing them with the value of 0.0195 obtained from DFT calculation for pure bcc-Fe [21], we found that for the Fe-rich FeCr alloy, this ratio is greater than in pure iron for all the Fe sites. It would be interesting to compare these DFT results with measurements performed using X-ray Magnetic Circular Dichroism (XMCD) that were recently performed over a range of Cr concentrations [22].

We note that the presence of an ordered phase $Fe_{15}Cr$ is consistent with experimental observations of short-range order (SRO) in the Fe-rich region [23], since it is well correlated with the local environment of Cr atoms discussed above. We have evaluated the SRO parameters in the Fe-rich region at temperature $T = 750$ K, close to the temperature at which experimental observations were performed (705 K). We found behaviour similar to that observed experimentally: the first and second NN parameters, which are negative and close to their theoretical minimum values at 5% Cr, become positive at 10.5% Cr [11]. There is a notable discrepancy at 15% Cr, where the predicted positive value of SRO is higher than the experimental values, indicating that the degree of Cr segregation in our model is much stronger than in the experiment. The reasons for this difference have to be investigated carefully. On the one hand, it

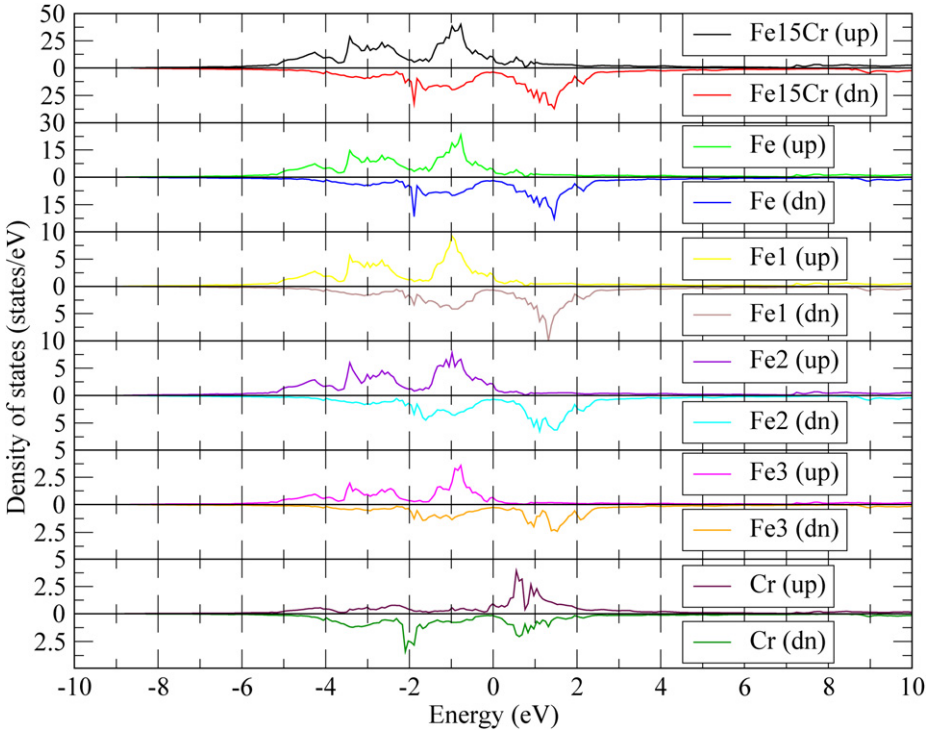

Fig. 3. Total and locate density of states calculated within collinear spin-polarized DFT calculations in $Fe_{15}Cr$ structure. The position of the Fermi energy corresponds to the origin of the energy axis.

Fig. 3. Densités d'état totale et sur certains sites de la structure $Fe_{15}Cr$, obtenues par calculs basés sur the fonctionnelle de la densité dans l'approximation de spins polarisés colinéaires.

Table 1
Averaged spin, orbital moments (in μ_B) and their ratios obtained from non-collinear spin-polarized DFT calculations for different crystallographic sites in $Fe_{15}Cr$

Tableau 1
Pour différents sites cristallographiques de la phase $Fe_{15}Cr$: spins moyens, moments orbitaux et leur rapport calculés à partir de la fonctionnelle de la densité dans l'approximation de spins polarisés non-colinéaires

Crystallographic site	$\langle M_s \rangle$	$\langle M_o \rangle$	$\langle M_o \rangle / \langle M_s \rangle$	E_f^{vac}	$E_f^{\langle 110 \rangle}$	$E_f^{\text{Fe–Cr}\langle 110 \rangle}$
(8g) Fe	2.2740	0.0553	0.0243	2.20	3.71	3.86
(3c) Fe1	2.2856	0.0547	0.0239	2.12	3.74	3.69
(3d) Fe2	2.4110	0.0573	0.0238	2.25	3.74	3.63
(1b) Fe3	2.5510	0.0600	0.0235	1.92	3.75	3.58
(1a) Cr	−1.6950	0.0090	−0.0053	2.18	4.09	3.63

The last three columns show the formation energy (in eV) of mono-vacancy, ⟨110⟩ dumbbell and ⟨110⟩ mixed Fe–Cr dumbbell calculated at these sites.

could be is associated with the accuracy of the present set of CE coefficients which have been obtained essentially by the DFT data base in Fe-rich region [13]. On the other hand, it could be linked with the equilibrium that is, in general, not reached within the present supercell exchange Monte Carlo simulation. Finally, as the precipitation is a kinetic process where the time plays an important role, experimental observation at different annealing time can show the different degree of order. As discussed in Section 4, our kinetic Monte Carlo simulation at 14% Cr, however, shows that the Cr cluster size increases at 14% Cr in comparison with the equilibrium configuration implying a greater degree of segregation rather than of ordering.

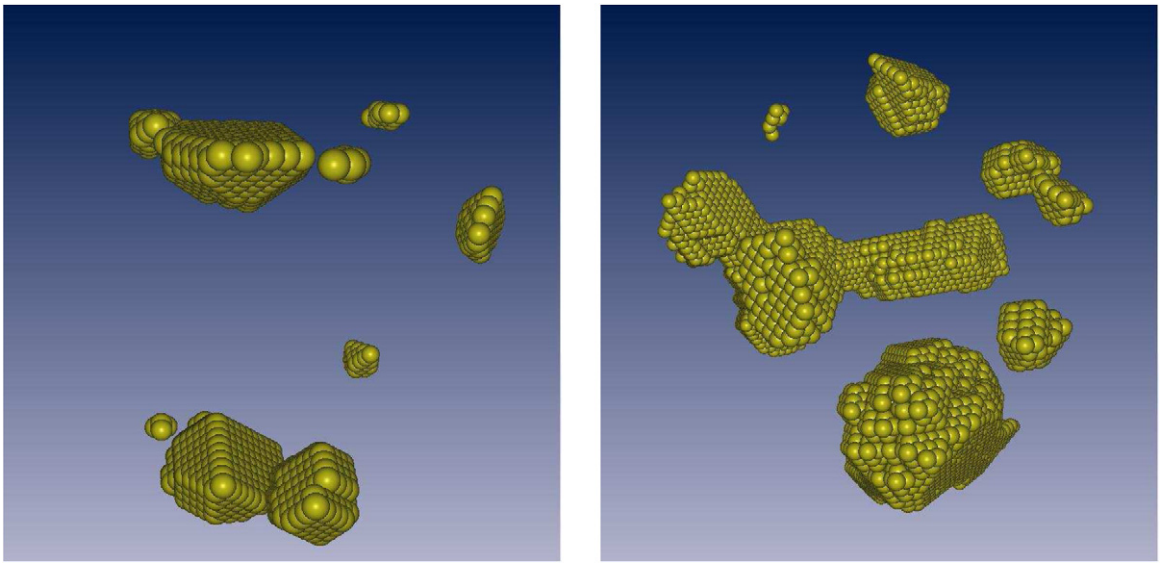

Fig. 4. Fe clusters obtained from CE study for Fe–Cr alloys with 2% Fe (left) and 10% Fe (right) at $T = 0$ K.

Fig. 4. Amas d'atomes de fer obtenus à 0 K à partir de la méthode de dévelopement en amas dans des alliages Fe–Cr avec 2 % (à gauche) et 10 % (à droite) de fer.

4. Cr clustering from kinetic Monte Carlo simulations

We used the exchange Monte Carlo technique to investigate the equilibrium phase diagram of Fe–Cr alloys [11]. The DFT-predicted lowest energy phase $Fe_{15}Cr$ is found to act as a precursor of thermodynamic behaviour at different temperatures and Cr concentrations. Clustering of Cr atoms begins at concentrations exceeding approximately 10% at 800 K and 20% at 1400 K with Cr–Fe interfaces being parallel to the [110] planes. Using the CE interactions, we calculated the interfacial energy for the three coherent interfaces ([110], [100] and [111]), and found it to have the lowest value in the [110] case (2.97 meV/Å^2, as compared to 9.7 meV/Å^2 for the [111] and 13.36 meV/Å^2 for the [100] interface). Fig. 4 shows Fe-rich clusters obtained in our simulations for 2% and 10% Fe at $T = 0$ K. (Cr atoms are not shown in this figure.) We see that in the Cr-rich region, the phase separation begins at the smallest concentrations of Fe in the α'-phase in a striking asymmetry with the situation in the Fe-rich region, where in the solid solution limit chromium atoms tend to stay away from each other. We note that the consolute temperature of the Fe–Cr phase diagram simulated in the present CE approximation lies between 1400 and 1600 K. This is higher than the values predicted by the CALPHAD method [15], and the disagreement is partially attributable to the absence of a vibrational entropy term in the cluster expansion and the limitations of the current set of CE coefficients. The incorporation of experimental data on the vibrational entropy of the Fe–Cr system [24] improves the agreement between our results and those of CALPHAD. The asymmetry of the Fe–Cr phase diagram taking into account the excess vibrational entropy contribution has also been discussed in [25] using the recently developed classical potentials for this alloy [7]. These authors also found the discrepancy in the critical temperature from high-temperature analysis comparison with the experimental data although their predicted vibrational entropy is somehow five time larger than the experimental value of 0.2 k_B at ≈50% Cr [24].

To investigate the kinetics of radiation induced segregation and precipitation in Fe–Cr binary alloys, we need to develop a comprehensive description of defect (vacancy and self-interstitial atom (SIA)) diffusion in the alloy. As a step towards this objective we have performed a systematic study of defect energetics in the ordered $Fe_{15}Cr$ phase with negative mixing enthalpy. The last three columns of Table 1 shows the vacancy, SIA ⟨110⟩ dumbbell and SIA ⟨110⟩ mixed dumbbell formation energies calculated by DFT for different Fe and Cr sites in this structure. In comparison with DFT data for pure elements [26,27] for vacancy (2.15 and 2.64 eV in bcc Fe and Cr, respectively) and ⟨110⟩ dumbbell formation energies (3.95 and 5.66 eV in bcc Fe and Cr, respectively), we found that the energy of a defect in Fe–Cr alloy depends on its environment. For instance, the vacancy formation energy at Cr site as well as the dumbbell ⟨110⟩ SIA formation energies at all the sites in $Fe_{15}Cr$ phase are reduced in comparison with those

Table 2
Migration barriers of vacancy exchange with Cr or Fe for different environments in 6 nearest neighbour sites of the saddle point configuration by Fe and Cr atoms in Fe-rich region

Tableau 2
Energie de migration d'une lacune lors de l'échange avec un atome de Cr, en fonction de différents environnements caractérisés par la nature des atomes, Fe or Cr, sur les 6 sites plus proches voisins de la position de col, dans la région riche en fer du diagramme de phases

Exchange atom	Environment	Energy barrier	Exchange atom	Environment	Energy barrier
Cr	6Fe	0.571	Fe	6Fe	0.640
Cr	5Fe + 1Cr	0.628	Fe	5Fe + 1Cr	0.627
Cr	4Fe + 2Cr	0.656	Fe	4Fe + 2Cr	0.646
Cr	3Fe + 3Cr	0.886	Fe	3Fe + 3Cr	0.696
Cr	2Fe + 4Cr	0.718	Fe	2Fe + 4Cr	0.678
Cr	1Fe + 5Cr	0.647	Fe	1Fe + 5Cr	0.655
Cr	6Cr	0.561	Fe	6Cr	0.635

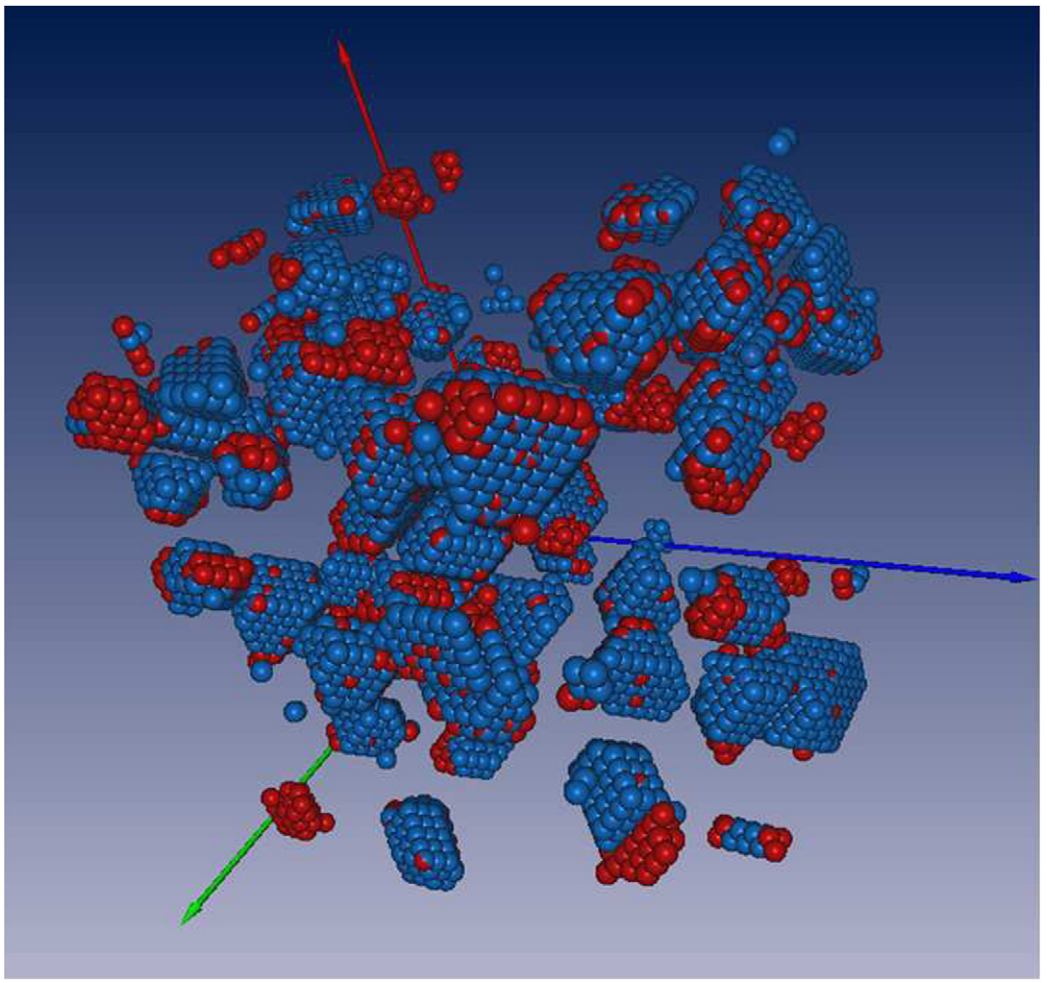

Fig. 5. Comparison of clustering of Cr atoms in 14% Cr alloy: results of an equilibration at $T = 200$ K (red) and those of a the subsequent kMC simulation carried out for $T = 300$ K with a single vacancy inserted in a cell of 128 000 sites (blue). The interval of time described by the simulation was 153 068 seconds.

Fig. 5. Formation d'amas de Cr dans un alliage Fe–Cr à 14 % de Cr. On fait subir au système à l'équilibre thermique à $T = 200$ K (les atomes de Cr sont en rouge) une simulation de type Monte Carlo cinétique faite à 300 K avec une seule lacune dans la cellule de simulation qui contient 128 000 sites. Les atomes bleus représentent les atomes de Cr après cette simulation à 300 K. L'intervalle de temps décrit par la simulation était de 153 068 secondes.

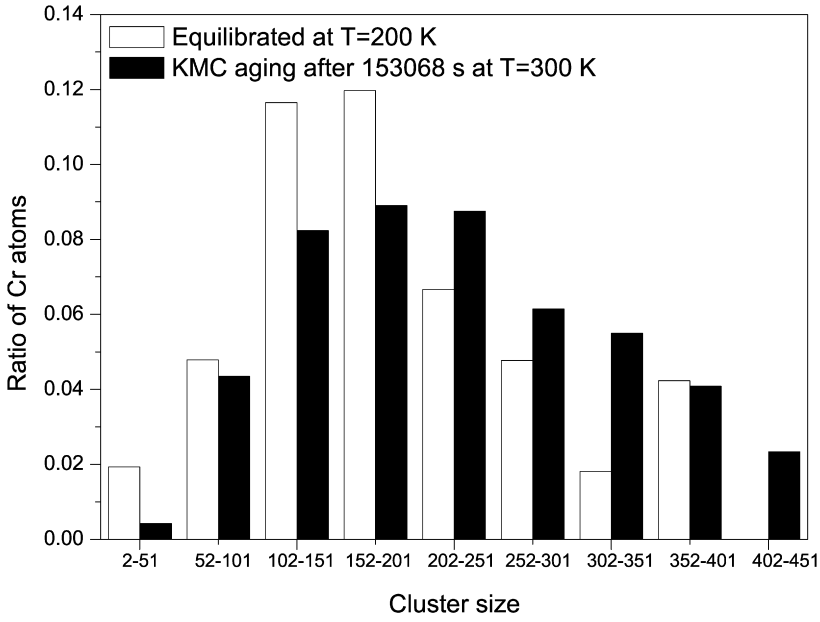

Fig. 6. Ratios of Cr atoms in clusters of given size with respect to the total number of Cr atoms in 14% Cr alloy.

Fig. 6. Rapport entre le nombre d'atomes de Cr dans les amas et le nombre total d'atomes de Cr dans un alliage Fe–Cr à 14 % de Cr.

in pure elements. In connection with the study of the mixed ⟨110⟩ dumbbell configuration, it is interesting to analyse the formation energy at site Fe3 (3.58 eV) and Cr (3.63 eV) where, as it is shown in Fig. 2, their environment until 4NN and 5NN is comprised of Fe atoms in comparison with those in the corresponding ⟨110⟩ dumbbell one (3.75 and 4.09 eV, respectively). Our prediction of lower mixed dumbbell formation energies agrees with the electrical resistivity recovery measurements in dilute Fe–Cr alloys for which one would expect that trapped mixed dumbbell defects become mobile at temperatures below the onset of long-range SIA's migration in bcc-Fe [28].

The challenge in modelling precipitation kinetics in concentrated alloys is related to the problem of environmental dependence of migration energy barriers of defects [29]. These barriers have to be computed for various configurations corresponding to a different repartition of Fe and Cr atoms among the nearest neighbours of the saddle-point positions. Table 2 shows results of DFT calculations for vacancy migration energies (in eV units) calculated at the saddle point in the Fe-rich region. The mono-vacancy migration energy in pure bcc-Fe is 0.64 eV whereas the migration energy for a vacancy exchanging with a Cr atom in bcc-Fe is 0.57 eV. We have used these two DFT data as starting values to perform preliminary kinetic Monte Carlo (kMC) simulations. The results from Table 2 show that the vacancy migration barriers are maximum for both Cr and Fe exchanges with vacancy when there are 3Cr and 3Fe atoms occupying 6NN position of the saddle-point position.

Atomistic kMC has been used to study phase transformation kinetics during thermal ageing or irradiation [30]. Diffusion proceeds by migration of point defects (for example vacancies), occurring with frequency

$$\Gamma_{\mathrm{AV}} = \nu_A^0 \exp(-\Delta E_{\mathrm{AV}}^{\mathrm{mig}}/k_B T) \tag{3}$$

where $\Delta E_{\mathrm{AV}}^{\mathrm{mig}}$ is the migration barrier and ν_A^0 is the attempt frequency factor. The migration barrier is computed as

$$\Delta E_{\mathrm{AV}}^{\mathrm{mig}} = E_{\mathrm{AV}}^{\mathrm{mig}}(\mathrm{DFT}) + (1/2)(E_{\mathrm{AV}}^{I} - E_{\mathrm{VA}}^{F}) \tag{4}$$

where $E_{\mathrm{AV}}^{\mathrm{mig}}(\mathrm{DFT})$ denotes DFT migration energy calculated at the saddle point position for vacancy exchange with a Fe or a Cr atom. E_{AV}^{I} and E_{VA}^{F} are the initial and final energy, respectively, of the system with a vacancy exchange with an atom A. They are computed within the framework of a rigid lattice model using the set of CE interaction energies. Fig. 5 shows the preliminary result for 14% Cr alloy simulated by kMC in the presence of a single vacancy inserted in the super-cell ($40 \times 40 \times 40$) of bcc lattice with 128 000 sites. This initial configuration is created from an equilibrated alloy configuration in the presence of a vacancy at $T = 200$ K. The final configuration is obtained from kMC simulation after performing more than 10^8 Monte Carlo moves, or 153 068 seconds. Fig. 6 shows a comparison

of Cr cluster sizes in 14% Cr alloy before and after vacancy-mediated kMC simulations. It shows that during the kMC ageing, the ratios of Cr atoms in larger cluster size increases in comparison with the initial configuration obtained by exchange Monte Carlo simulations.

5. Conclusions

In this study we have shown that CE interactions obtained from DFT data base for binary Fe–Cr alloys are capable of accurately predicting thermodynamic, nano-clustering, short-range order, spin-polarized electronic structure and defect properties across a range of Cr concentrations. The preliminary result of modelling precipitation kinetics in the presence of a single vacancy appears promising, although there are still two remaining challenging issues. The first is related to the need to include the magnetic contribution to the total energy of the Fe–Cr alloy. It is now well established that the magnetic contribution to the total energy is crucial for distinguishing the SIA defect behaviour between magnetic and non-magnetic bcc transition metals [27,31]. The second issue is related to the problem of long-range nature of the conventional CE approximation that for Fe–Cr alloys require the inclusion of up to 5NN pairwise and many-body interactions. With such complex interactions, it is very difficult to simulate kinetics of precipitation realistically for large length and time scales. In order to overcome these two problems, it is necessary to develop a new approach to coupling short-ranged magnetic and non-magnetic interaction parameters, possibly involving a more complete DFT database for both magnetic and non-magnetic configurations of Fe–Cr binary alloy. We expect that the formalism will involve elements of the tight-binding Stoner model [3,32] and ideas related to the development of the magnetic potential [4,5]. The fact that a suitable short-range formalism may indeed be devised is also supported by the recent work of Moran et al. [33] who showed that in ferromagnetic bcc-Fe the 1NN and 2NN interactions in the Heisenberg model for bcc-Fe are much more dominant than the 3NN and 4NN interactions.

Acknowledgements

We would like to thank V. Blum, J.-L. Boutard, A. Caro, E. Clouet, R. Drautz, L. Malerba, P.A. Miodownik, P. Olsson, M. Victoria and B. Wirth for many stimulating discussions. This work, supported by the United Kingdom Engineering and Sciences Research Council and European Communities under the contract of association between EURATOM and UKAEA, was carried out within the framework of the European Fusion Development Agreement (Task No. D051-TW6-TTMS-007). The views and opinions expressed herein do not necessarily reflect those of the European Commission.

References

[1] A. Koyama, A. Hishinuma, D.S. Gelles, R.L. Klueh, W. Dietz, K. Ehrlich, J. Nucl. Mater. 233–237 (1996) 138.
[2] E.A. Little, D.A. Stow, J. Nucl. Mater. 87 (1979) 25.
[3] D. Nguyen-Manh, V. Vitek, A.P. Horsfield, Prog. Mater. Sci. 52 (2007) 255.
[4] S.L. Dudarev, P.M. Derlet, J. Phys.: Condens. Matter 17 (2005) 7097.
[5] P.M. Derlet, S.L. Dudarev, Prog. Mater. Sci. 52 (2007) 299.
[6] P. Olsson, I.A. Abdrikosov, I. Vitos, J. Wallenius, J. Nucl. Mater. 321 (2003) 84–90.
[7] A. Caro, D.A. Crowson, M. Caro, Phys. Rev. Lett. 95 (2005) 075702.
[8] A. Zunger, in: P.E.A. Turchi, A. Gonis (Eds.), Proceedings of the NATO ASI on "Statics and Dynamics of Alloy Phase Transformations", Plenum Press, New York, 1994, p. 361.
[9] V. Blum, A. Zunger, Phys. Rev. B 69 (2004) 020103(R).
[10] R. Drautz, A. Diaz-Ortiz, M. Fähnle, Phys. Rev. Lett. 93 (2004) 067202.
[11] M. Lavrentiev, R. Drautz, D. Nguyen-Manh, P.T.C. Klaver, S.L. Dudarev, Phys. Rev. B 75 (2007) 014208.
[12] D. Nguyen-Manh, M.Yu. Lavrentiev, S.L. Dudarev, in: P. Gumbsch (Ed.), "Multiscale Materials Modeling", Third International Conference, September 2006, Freiburg, Germany, pp. 767–770; J. Comp. Mater. Design (2007).
[13] P.T.C. Klaver, R. Drautz, M.W. Finnis, Phys. Rev. B 74 (2006) 224207.
[14] F. Ducastelle, in: Order and Phase Stability in Alloys, Elsevier, 1991.
[15] N. Saunders, A.P. Miodownik, in: CALPHAD, Calculation of Phase Diagrams, Pergamon, 1998.
[16] M. Hennion, J. Phys. F: Met. Phys. 13 (1983) 2351.
[17] A.A. Mirzoev, M.M. Yalalov, D.A. Mirzaev, Phys. Met. Metallogr. 97 (2004) 4336.
[18] P. Olsson, I.A. Abrikosov, J. Wallenius, Phys. Rev. B 73 (2006) 104416.
[19] D. Nguyen-Manh, M.Yu. Lavrentiev, S.L. Dudarev, Comp. Mat. Sci. (2007).
[20] G. Kresse, J. Furthmüller, in: VASP the GUIDE, Universität Wien, Austria, 2003.

[21] G.Y. Guo, H. Ebert, Phys. Rev. B 50 (1994) 3861.
[22] A. Froideval, M. Samaras, M. Victoria, W. Hoffelner, Abstract No. JJ3.6, MRS Fall Meeting, November, Boston, 2006.
[23] I. Mirebeau, M. Hennion, G. Parette, Phys. Rev. Lett. 53 (1984) 687.
[24] B. Fultz, L. Anthony, J.L. Robertson, R.M. Nicklow, S. Spooner, M. Mostoller, Phys. Rev. B 52 (1995) 3280.
[25] A. Caro, M. Caro, E.M. Lopasso, D.A. Crowson, Appl. Phys. Lett. 89 (2006) 121902.
[26] C.C. Fu, F. Willaime, P. Ordejon, Phys. Rev. Lett. 92 (2004) 175503.
[27] D. Nguyen-Manh, A.P. Horsfield, S.L. Dudarev, Phys. Rev. B 73 (2006) 020101R.
[28] A.L. Nikolaev, J. Phys.: Condens. Matter 11 (1999) 8633.
[29] Y. Le Bouar, F. Soisson, Phys. Rev. B 65 (2003) 094103.
[30] G. Martin, P. Bellon, F. Soisson, Defect and Diffusion Forum 143 (1997) 385.
[31] P.M. Derlet, D. Nguyen-Manh, S.L. Dudarev, Phys. Rev. B 76 (2007) 054107.
[32] G.Q. Liu, D. Nguyen-Manh, B.G. Liu, D.G. Pettifor, Phys. Rev. B 71 (2005) 174115.
[33] S. Moran, C. Ederer, M. Fähnle, Phys. Rev. B 67 (2003) 012407.